

# The Throughput of Underwater Networks: Analysis and Validation using a Ray Tracing Simulator

Kostas Stamatou, *Member, IEEE*, Paolo Casari, *Member, IEEE*, and Michele Zorzi, *Fellow, IEEE*

**Abstract**—We propose a theoretical framework to evaluate the expected throughput of underwater networks over an ensemble of node topologies and propagation environments. The analysis is based on the assumptions that the transmitters are spatially distributed according to a Poisson point process, and that the channel follows a Rayleigh fading distribution, with a mean that is determined by spreading loss and frequency-dependent absorption. We evaluate the probability of a successful transmission, i.e., the probability that the signal-to-interference-and-noise ratio at the typical receiver is greater than a given threshold, and determine the maximum network throughput density over the transmitter density and the operating frequency. The theoretical results are validated using a realistic underwater channel simulator based on ray tracing. It is demonstrated that, for a number of practical scenarios, the theoretical and simulated throughput match provided that the spreading-loss exponent is appropriately fitted to the simulation scenario. Overall, the proposed framework provides easy-to-obtain network throughput results, which can be used as a complement or an alternative to time-costly, deployment-dependent network simulations.

**Index Terms**—Underwater networks, throughput, transmission capacity, Poisson point process, Urick model, ray tracing, Bellhop.

## I. INTRODUCTION

The field of underwater (UW) networking has undergone significant development in recent years and now encompasses a wide variety of applications [1]. Early research in the field [2], [3], and later testbed deployments [4], have demonstrated the feasibility of UW networks in practice. Primarily, the attention of the research community has been focused on physical-layer and hardware design, channel characterization [1], as well as protocol design, comparison and evaluation [5]–[8]. In contrast, only a limited number of papers have addressed the analytical performance evaluation of UW networks and the derivation of fundamental performance limits. In this light, this paper presents a theoretical framework for evaluating the throughput of UW networks, which does not

depend on the deployment topology, and captures with closed-form expressions the main effects of the UW propagation environment on the overall network performance. The validity of the proposed approach is confirmed via detailed ray tracing simulations for various operational scenarios.

On the theoretical research front, [9] determined the communication-bandwidth/distance relationship and the ergodic capacity for a single UW link, using the empirical Urick acoustic channel model [10]. In [11], the bandwidth-distance relationship of [9] was employed to assess the tradeoff between delay and energy consumption in multi-hop UW networks with error control. The results in [9] were also extended in [12], for an UW cellular network with frequency reuse, and the tradeoff between the reuse factor and the maximum feasible user density was evaluated. On the one hand, [12] captured the fundamental tradeoff that exists between deploying more nodes in the same area and the resulting network interference. On the other hand, the assumption of a cellular structure is restrictive in view of the fact that, in typical UW network deployments, the node topology does not obey a particular structure, mainly due to the difficulty and cost of placing nodes at particular locations [13]. In [14], employing asymptotic arguments, the authors showed that the amount of information that can be exchanged by each source-destination link in an UW network goes to zero as  $n^{-1/b}$ , where  $n$  is the number of nodes and  $b$  is the spreading-loss exponent. In the same vein, [15] considered a multi-hop underwater network with regular geometry and showed that nearest-neighbor routing is order-optimal, if the carrier frequency scales appropriately with the number of nodes. The drawback of [14], [15] is that, although they reveal the scaling behavior of an UW network, they do not provide the preconstants of the scaling laws, which may vary widely depending on the channel and network parameters.

In this paper, we take a different approach compared to the aforementioned work. We consider an UW network where the transmitters are randomly distributed in space according to a homogeneous Poisson point process (PPP) of a given density. This model has been widely employed for the performance analysis of wireless radio networks; the reader is referred to [16], [17] for a comprehensive overview of existing results and an exhaustive list of references. The main advantages of the model are its generality, since it allows us to consider an ensemble of network topologies without being limited by a particular configuration, and the analytical tractability of the Poisson distribution.

We derive the success probability for the typical transmitter-receiver (TX-RX) link over different TX locations and channel gain realizations. The analysis is based on the assumption that

Manuscript received February 16, 2012; revised June 5, 2012; revised November 14, 2012; accepted November 29, 2012. The associate editor coordinating the review of this paper and approving it for publication was T. Zemen.

Part of this work was presented at the IEEE GLOBECOM 2011 Conference, Houston, TX, USA. This work has been supported in part by the Italian Institute of Technology within the Project SEED framework (NAUTILUS project), by the European Commission under the 7th Framework Programme (grant agreement no. 258359-CLAM), and by the US Office of Naval Research under grant N00014-14-01422.

Kostas Stamatou is with CTTC, Av. Carl Friedrich Gauss 7, 08860 Castelldefels, Spain (e-mail: kostas.stamatou@cttc.es). Paolo Casari and Michele Zorzi are with the Department of Information Engineering, University of Padova, Via Gradenigo 6/B, 35131 Padova, Italy, and with Consorzio Ferrara Ricerche, via Saragat 1, 44122 Ferrara, Italy (e-mail: {paolo.casari, michele.zorzi}@dei.unipd.it).

Digital Object Identifier XX.XXXX/T-WC.2012.XXXXXX

the received power is exponentially distributed, with a mean which depends on the spreading loss and frequency-dependent absorption according to the Urick model [10, Ch. 5]. The expression can be easily calculated numerically and captures the dependence of the success probability on key parameters such as the transmission distance, the spreading-loss exponent and the operating frequency. We then maximize the *network throughput density* over the TX density and the operating frequency, and demonstrate that the throughput-maximizing frequency is 2 to 4 times larger than the frequency which maximizes the link signal-to-noise-ratio (SNR), providing up to a seven-fold improvement in the respective throughput. This is due to the frequency-dependent absorption of the interfering signals, which allows for a higher density of transmitting nodes. In addition, we calculate the maximum supportable density of TXs such that a given constraint on the success probability is satisfied, i.e., the *transmission capacity* of the UW network [17]. The constraint expresses the stringency of the link performance requirement and depends on the application. Given the energy constraints of UW nodes, as well as the large delay penalties associated with retransmissions, imposing a constraint on the success probability and deriving the respective transmission capacity are particularly relevant to the operation of UW networks. Overall, the single-hop results derived in the paper can be used as a starting point for the analysis of multi-hop UW networks, as was done, e.g., in [18] for the case of terrestrial networks.

The second part of the paper is devoted to the validation of the analysis, by means of simulations of a realistic UW environment performed with the Bellhop ray tracing software [19]. We focus on a shallow UW network scenario at a depth of 100 m, for which it is demonstrated that the received signal power distribution, over several realizations of the sound speed profile (SSP), can in most cases be approximated as exponential. First, a curve-fitting step is performed for a single TX-RX link, wherein the spreading-loss exponent is selected such that the empirical mean received power best matches the one simulated with Bellhop. Then, employing the fitted spreading-loss exponent, it is shown that the theoretical and simulated throughput match for a wide range of transmission distances and operating frequencies.

The remainder of the paper is organized as follows. In Section II, we describe the theoretical system model in detail. In Section III, we evaluate analytically the success probability and the related network metrics, and in Section IV we provide numerical examples. Our simulation campaign is described in detail in Section V. Section VI concludes the paper and discusses directions for future research.

## II. THEORETICAL MODEL

We consider an UW network that consists of an infinite number of TXs, which are distributed on the plane ( $d = 2$  dimensions) or in space ( $d = 3$ ) according to a PPP  $\Phi = \{x\}$  of density  $\lambda$ , where  $x$  denotes location. Each TX has a RX at distance  $R > 0$  and a random orientation, and transmits at a constant power  $P$  (henceforth, the symbol  $R$  is reserved to denote the distance between a TX and its *intended* receiver).

The more complicated case of random link distances can also be handled and is presented separately in Section III-C. The channel power gain at frequency  $f$  between a generic TX/RX pair at distance  $r$  consists of (a) the distance-dependent term  $r^{-b}a(f)^{-r}$  where, typically,  $b \geq 1$ , and  $a(f) > 1$  is the absorption factor, and (b) fading  $h(f)$ , where  $h(f)$  is assumed to be exponentially distributed with unit mean (or  $\sqrt{h(f)}$  is Rayleigh distributed<sup>1</sup>). The fading random variables are spatially independent and identically distributed. Moreover, we assume the presence of noise, which is additive with a power spectral density  $W(f)$ . For generally accepted empirical functions  $W(f)$  and  $a(f)$ , the reader is referred to [9], [10] and the references therein.<sup>2</sup> Henceforth, we refer to the distance-dependent gain  $r^{-b}a(f)^{-r}$  as the ‘‘Urick model’’ and to the parameter  $b$  as the spreading-loss exponent.

As in [12], [21]–[23], we assume narrowband transmission, i.e., transmission in a ‘‘small’’ bandwidth  $\delta f$  around the carrier frequency  $f_o$ . Within  $\delta f$ , we assume that  $W(f) = W(f_o)$ ,  $a(f) = a(f_o)$  and  $h(f) = h(f_o)$  (where  $h(f_o)$  is a random quantity).<sup>3</sup> In the following, the dependence of  $W$  and  $a$  on  $f_o$  is implied.

Without loss of generality due to the structure of the PPP, let the RX of the typical TX be located at the origin. The signal-to-interference-and-noise-ratio seen at this RX is

$$\text{SINR} = \frac{h_{x_0} R^{-b} a^{-R}}{W \delta f / P + I}, \quad (1)$$

where  $I$  is the (normalized with respect to  $P$ ) interference power

$$I = \sum_{x \in \Phi \setminus \{x_0\}} h_x \|x\|^{-b} a^{-\|x\|}, \quad (2)$$

and  $h_x$  denotes the fading coefficient between the TX located at  $x$  and the RX;  $\|\cdot\|$  is the norm of  $x$ ; and  $x_0$  is the position of the typical TX, which is excluded from the set of interferers. We define the success probability,  $P_s$ , as the probability that the SINR satisfies a predetermined constraint  $\theta$ , i.e.,

$$P_s = \mathbb{P}(\text{SINR} \geq \theta), \quad (3)$$

over all TX topologies and fading realizations. Taking an information-theoretic viewpoint, if  $\text{SINR} \geq \theta$  is satisfied, and the noise, as well as the interference (given its power) are assumed to be Gaussian, then a rate of  $\log_2(1 + \theta)$  (bits/symbol) is achievable. Similarly to the case of wireless radio networks [16], we define the throughput density (or density of successful transmissions)  $\tau(\lambda) = \lambda P_s(\lambda)$ , which captures the tradeoff between the density of transmissions in space and the individual link quality; the maximum TX density

<sup>1</sup>There exists experimental evidence that the Rayleigh distribution models the medium-range shallow water channel accurately [20]. In any case, in Section V it is demonstrated that this modeling assumption is not crucial, and that the analysis predicts the simulated throughput even when the simulated channel distribution departs from the exponential model.

<sup>2</sup>In this paper, we set  $W(f)$  as in [9, eq. (6)], and  $\log_{10} a(f) = (40f^2 / (4100 + f^2) + 0.1f^2 / (1 + f^2)) / 914.4$  dB/m, as also implemented in the Bellhop software [19].

<sup>3</sup>The case of wideband transmission can be handled by splitting the available bandwidth in sub-bands and applying the analysis of Section III to each sub-band. A more detailed analysis of the wideband case represents a substantial extension and is left for future work.

$\lambda_\varepsilon$  such that the constraint  $P_s \geq 1 - \varepsilon$  is satisfied; and the transmission capacity  $c_\varepsilon = \lambda_\varepsilon(1 - \varepsilon)$ , i.e., the throughput density resulting from the maximum TX density under the particular constraint. In the next section we obtain exact expressions and bounds for  $P_s$ ,  $\tau(\lambda)$  and  $c_\varepsilon$ .

### III. ANALYTICAL EVALUATION OF THE SUCCESS PROBABILITY AND NETWORK METRICS

In order to evaluate the success probability defined in (3), we follow the approach outlined in [16] for the case of wireless radio networks. The main difference is the nature of the path-loss model of UW signal propagation, which results in a different expression for  $P_s$ .

#### A. Success probability

Since  $h_{x_0}$  is exponentially distributed,  $P_s$  can be written as [16, Eq. (9)]

$$P_s = \exp\left(-\frac{\theta R^b a^R W \delta f}{P}\right) \mathcal{L}_I(\theta R^b a^R) \triangleq P_{s,n} P_{s,i}, \quad (4)$$

where  $\mathcal{L}_I(s)$ ,  $s > 0$ , is the Laplace transform of the probability density function of the interference, and  $P_{s,n}$ ,  $P_{s,i}$  denote the success probabilities taking into account only noise and interference, respectively. When  $P \rightarrow \infty$  (and all other parameters are kept constant), the network is interference-limited and  $P_s = P_{s,i}$ . Since  $\Phi$  is a PPP, it is known that [24, Eq. (2.2), p. 292] (see also [16, Eq. (8)])

$$\mathcal{L}_I(s) = \exp\left(-\int_0^{+\infty} \mathbb{E}_h\left[1 - e^{-shr^{-b}a^{-r}}\right] \lambda_d(r) dr\right), \quad (5)$$

where  $\lambda_d(r) \triangleq \lambda c_d r^{d-1}$  and  $c_d = \text{Vol}(B_d(0,1))$  is the volume of the  $d$ -dimensional unit ball. For  $d = 2$  we have  $\lambda_2(r) = 2\lambda\pi r$ , and for  $d = 3$  we have  $\lambda_3(r) = 4\lambda\pi r^2$ . In the extreme case where  $a = 1$ , i.e., there is no absorption,  $\mathcal{L}_I(s)$  is defined as long as  $b > d$  [16]. This case corresponds to a wireless radio network and has been well studied in the literature [16]. In the following, we extend the analysis to  $a > 1$ , which is pertinent to UW acoustic communication. Since  $\mathbb{E}_h[e^{-sh}] = (1+s)^{-1}$ , from the definition of  $P_{s,i}$  and (5), we obtain

$$P_{s,i} = \exp\left(-\lambda c_d \int_0^{+\infty} \frac{dr^{d-1}}{1 + \frac{r^b a^r}{\theta R^b a^R}} dr\right). \quad (6)$$

The integral in the exponent does not have a general closed-form expression, but can be written as an infinite series of known functions, as shown in the following proposition. We recall the definitions of the upper incomplete Gamma function

$$\Gamma(\zeta, x) = \int_x^{+\infty} t^{\zeta-1} e^{-t} dt, \quad x > 0, \quad \zeta \in \mathbb{R}, \quad (7)$$

the Gamma function  $\Gamma(\zeta) \triangleq \Gamma(\zeta, 0)$ ,  $\zeta > 0$ , the confluent hypergeometric function [25, p. 1023]

$${}_1F_1(\zeta, \xi; x) = \frac{\Gamma(\xi)}{\Gamma(\zeta)\Gamma(\xi-\zeta)} \int_0^1 t^{\zeta-1} (1-t)^{\xi-\zeta-1} e^{tx} dt, \quad \xi > \zeta > 0, \quad x \in \mathbb{R}, \quad (8)$$

and the principal branch of the Lambert function  $\mathcal{W}(x)$ ,  $x \geq -e^{-1}$  [26], where  $\mathcal{W}(x)$  is the unique solution of  $ye^y = x$ ,  $y \geq -1$ .

**Proposition 1** *The success probability in the interference-limited regime is*

$$P_{s,i} = \exp\left(-\lambda c_d \sum_{n=0}^{\infty} (-1)^n A_n\right), \quad (9)$$

where

$$A_0 = \bar{R}^d + \frac{d\theta R^b a^R}{(\log a)^{d-b}} \Gamma(d-b, \bar{R} \log a), \quad (10)$$

$$A_n = \frac{d\bar{R}^d a^{-\bar{R}n}}{d+bn} {}_1F_1(d+bn, d+bn+1; \bar{R}n \log a) + \frac{d(\theta R^b a^R)^{n+1}}{((n+1)\log a)^{d-b(n+1)}} \Gamma(d-b(n+1), \bar{R}(n+1)\log a), \quad n \geq 1, \quad (11)$$

and

$$\bar{R} = \frac{b}{\log a} \mathcal{W}\left(\frac{\log a}{b} (\theta R^b a^R)^{1/b}\right). \quad (12)$$

*Proof:* Denote the integral in (6) by  $\mathcal{I}$ . Then

$$\mathcal{I} = d \int_0^{\bar{R}} \frac{r^{d-1}}{1 + \frac{r^b a^r}{\theta R^b a^R}} dr + d\theta R^b a^R \int_{\bar{R}}^{+\infty} \frac{(r^b a^r)^{-1} r^{d-1}}{1 + \frac{\theta R^b a^R}{r^b a^r}} dr, \quad (13)$$

where  $\bar{R}$  is such that  $\bar{R}^b a^{\bar{R}} = \theta R^b a^R$  or

$$\frac{\log a}{b} \bar{R} e^{\frac{\log a}{b} \bar{R}} = \frac{\log a}{b} (\theta R^b a^R)^{1/b}. \quad (14)$$

Applying the Lambert function to both sides of this equation results in (12). Employing the series expansion

$$\frac{1}{1+x} = \sum_{n=0}^{+\infty} (-x)^n, \quad |x| < 1, \quad (15)$$

in (13) yields

$$\mathcal{I} = d \sum_{n=0}^{\infty} (-1)^n (\theta R^b a^R)^{-n} \int_0^{\bar{R}} r^{d+bn-1} a^{rn} dr + d \sum_{n=0}^{\infty} (-1)^n (\theta R^b a^R)^{n+1} \int_{\bar{R}}^{+\infty} r^{d-b(n+1)-1} a^{-r(n+1)} dr. \quad (16)$$

From (16), (7) and (8), we obtain (9)-(11). ■

*Remarks on Proposition 1:*

1.  $\bar{R}$  in (12) is the *critical radius*, defined as the distance at which the power from an interferer (averaged over the fading) is equal to  $(\theta R^b a^r)^{-1}$ , or  $\bar{R}^b a^{\bar{R}} = \theta R^b a^R$ . Alternatively, if we ignore fading, any interferer within a ball of this radius around the typical RX can cause an outage. By definition, if  $\theta \geq 1$ , then  $\bar{R} \geq R$ , and the equality holds for  $\theta = 1$ . If  $\theta \rightarrow \infty$  (high-rate transmission) then  $\bar{R} \rightarrow \infty$ . With respect to the dependence of  $\bar{R}$  on the absorption factor, we have that,

if  $a \rightarrow 1$ , then  $\bar{R} \rightarrow \theta^{1/b}R$ . For  $a \rightarrow \infty$ , with the application of de l'Hôpital's rule, (12) results in

$$\begin{aligned} \lim_{a \rightarrow \infty} \bar{R} &= \lim_{a \rightarrow \infty} \frac{b}{\log a} \mathcal{W} \left( \frac{\log a}{b} (\theta R^b a^R)^{1/b} \right) \\ &\stackrel{(a)}{=} \lim_{a \rightarrow \infty} \frac{ba e^{-\mathcal{W} \left( \frac{\log a}{b} (\theta R^b a^R)^{1/b} \right)}}{1 + \mathcal{W} \left( \frac{\log a}{b} (\theta R^b a^R)^{1/b} \right)} \times \\ &\quad \times \frac{(\theta R^b)^{1/b}}{b} \left( a^{R/b-1} + \frac{R}{b} a^{R/b-1} \log a \right) \\ &\stackrel{(b)}{=} \lim_{a \rightarrow \infty} \frac{(\theta R^b a^R)^{1/b} (1 + \frac{R}{b} \log a)}{\frac{\log a}{b} (\theta R^b a^R)^{1/b}} \\ &= R, \end{aligned} \quad (17)$$

where (a) is due to the fact that the derivative of the Lambert function is

$$\mathcal{W}'(x) = \frac{e^{-\mathcal{W}(x)}}{1 + \mathcal{W}(x)}, \quad x > e^{-1},$$

obtained by differentiating  $\mathcal{W}(x)e^{\mathcal{W}(x)} = x$  with respect to  $x$ , and (b) is due to the fact that  $\lim_{a \rightarrow \infty} \mathcal{W} \left( \frac{\log a}{b} (\theta R^b a^R)^{1/b} \right) = +\infty$ .

2. Since the TX locations are obtained from a PPP,  $P_{s,i}$  in (6) is equal to the probability that there are no TXs within a ball of volume

$$V_d = c_d \sum_{n=0}^{+\infty} (-1)^n A_n. \quad (18)$$

3. Eq. (6) is defined for *any* positive value of  $b$ . In addition, employing Campbell's theorem [16], the mean interference power at the typical RX is

$$\begin{aligned} \mathbb{E}[I] &= \lambda c_d d \int_0^{+\infty} r^{d-b-1} a^{-r} dr \\ &= \lambda c_d d \Gamma(d-b) (\log a)^{b-d}, \end{aligned} \quad (19)$$

which is defined for  $b < d$ , while, for  $b \geq d$ ,  $\mathbb{E}[I] = \infty$ , due to the singularity of the path-loss law at the origin. Note that, in the case of terrestrial radio networks with path-loss law  $r^{-b}$ , the mean interference power is always infinite [16]. The difference between the two systems lies in the absorption factor  $a > 1$ , which, in the case of an UW network, ensures that the contribution of the far-away interferers in the TX PPP goes to zero exponentially with distance.

From Campbell's theorem, we also obtain

$$\begin{aligned} \mathbb{E}[I_{\text{far}}] &= \lambda c_d d \int_{\bar{R}}^{+\infty} r^{d-b-1} a^{-r} dr \\ &= \lambda c_d d \Gamma(d-b, \bar{R} \log a) (\log a)^{b-d}, \end{aligned} \quad (20)$$

where  $I_{\text{far}}$  is the total interference power from TXs located outside the ball of radius  $\bar{R}$  around the typical RX. Consequently, the second term in (10) is proportional to the ratio of the average interference power from "far" interferers to the average (over the fading) received signal power. From (9), (10) and (20), a "first-order" approximation to  $P_{s,i}$  is therefore

$$P_{s,i} \approx \exp(-\lambda c_d \bar{R}^d - \theta \text{SIR}_{\text{far}}^{-1}), \quad (21)$$

where  $\text{SIR}_{\text{far}} \triangleq R^{-b} a^{-R} / \mathbb{E}[I_{\text{far}}]$  is defined as the ratio of the average received power over the mean power of the far interferers.

In the following corollary, we obtain arbitrarily tight bounds to  $P_{s,i}$ , that involve only a finite number of terms in the series in (9).

**Corollary 1** *The success probability in the interference-limited regime is bounded as*

$$\exp\left(-\lambda c_d \sum_{n=0}^N (-1)^n A_n\right) < P_{s,i} < \exp\left(-\lambda c_d \sum_{n=0}^{N-1} (-1)^n A_n\right), \quad (22)$$

for any even integer  $N > 0$ . Moreover

$$\exp(-\lambda c_d A_0) < P_{s,i} < \exp\left(-\frac{\lambda c_d A_0}{2}\right). \quad (23)$$

*Proof:* For  $x \in (0, 1)$ ,

$$\frac{1}{1+x} = \sum_{n=0}^{N-1} (-x)^n + \sum_{n=N}^{+\infty} (-x)^n.$$

However,

$$\sum_{n=N}^{+\infty} (-x)^n = \frac{(-x)^N}{1+x} \leq 0,$$

which is  $> 0$  for  $N$  even and  $< 0$  for  $N$  odd. Therefore, for  $N$  even

$$\sum_{n=0}^{N-1} (-x)^n < \frac{1}{1+x} < \sum_{n=0}^N (-x)^n. \quad (24)$$

From (24) and (13), we obtain (22), following the same procedure as in the proof of Proposition 1. Eq. (23) is proved similarly by employing the trivial bounds  $1/2 < 1/(1+x) < 1$ , for  $x \in (0, 1)$ . ■

We close this section by deriving the limit of  $P_{s,i}$  for  $a \rightarrow \infty$ .

**Proposition 2** *For the interference-limited success probability defined in (6), we have that*

$$\lim_{a \rightarrow \infty} P_{s,i} = e^{-\lambda c_d R^d}. \quad (25)$$

*Proof:* It suffices to show that  $\lim_{a \rightarrow +\infty} \mathcal{I} = R^d$ , where  $\mathcal{I}$  is defined in (13). Assuming  $\theta \geq 1$ , i.e.,  $\bar{R} \geq R$ , the limit of the first term of (13) is

$$\begin{aligned} \lim_{a \rightarrow +\infty} &\left( \int_0^R \frac{dr^{d-1}}{1 + \frac{r^b a^r}{\theta R^b a^R}} dr + \int_R^{\bar{R}} \frac{dr^{d-1}}{1 + \frac{r^b a^r}{\theta R^b a^R}} dr \right) \\ &= \int_0^R \lim_{a \rightarrow +\infty} \frac{dr^{d-1}}{1 + \frac{r^b a^r}{\theta R^b a^R}} dr, \\ &= \int_0^R dr^{d-1} \\ &= R^d, \end{aligned}$$

since  $\lim_{a \rightarrow \infty} \bar{R} = R$  and the integrand is upper bounded for all  $a > 0$  by  $dr^{d-1}$ . Using similar arguments, the limit of the

second term of (13) is

$$\begin{aligned}
& \lim_{a \rightarrow +\infty} a^R \int_{\bar{R}}^{+\infty} \frac{(r^b a^r)^{-1} r^{d-1}}{1 + \frac{\theta R^b a^R}{r^b a^r}} dr \\
&= \lim_{a \rightarrow +\infty} \left( \int_R^{+\infty} \frac{r^{d-b-1} a^{R-r}}{1 + \theta \left(\frac{R}{r}\right)^b a^{R-r}} dr \right. \\
&\quad \left. - \int_R^{\bar{R}} \frac{r^{d-b-1} a^{R-r}}{1 + \theta \left(\frac{R}{r}\right)^b a^{R-r}} dr \right) \\
&= \int_R^{+\infty} \lim_{a \rightarrow +\infty} \frac{r^{d-b-1} a^{R-r}}{1 + \theta \left(\frac{R}{r}\right)^b a^{R-r}} dr \\
&= 0.
\end{aligned}$$

The case  $\theta < 1$  ( $R > \bar{R}$ ) can be handled similarly. This concludes the proof of (25).  $\blacksquare$

Proposition 2 implies that, in the limit of a large absorption factor  $a$ ,  $P_{s,i}$  is equal to the probability that there are no interferers within a ball of radius  $R$  around the typical RX.

### B. Network metrics

From the definition of  $\tau(\lambda)$ , (4), and Proposition 1, we have

$$\tau(\lambda) = \lambda \exp \left( -\lambda V_d - \frac{\theta R^b a^R W \delta f}{P} \right). \quad (26)$$

Optimizing over the density of TXs  $\lambda$ , the optimal throughput density is

$$\tau_o = \frac{1}{V_d} \exp \left( -\frac{\theta R^b a^R W \delta f}{P} - 1 \right), \quad (27)$$

where  $V_d$  is as in (18). Similarly, from the definition of the transmission capacity, we obtain that

$$c_\varepsilon = \max \left\{ \frac{1-\varepsilon}{V_d} \left( -\log(1-\varepsilon) - \frac{\theta R^b a^R W \delta f}{P} \right), 0 \right\}. \quad (28)$$

Note that  $c_\varepsilon > 0$  if

$$R^b a^R < \frac{-P \log(1-\varepsilon)}{\theta W \delta f}.$$

If we solve over  $R$ , we find that the maximum supportable transmission distance given  $\varepsilon$  is

$$R_{\max,\varepsilon} = \frac{b}{\log a} \mathcal{W} \left( \frac{\log a}{b} \left( -\frac{P \log(1-\varepsilon)}{\theta W \delta f} \right)^{1/b} \right). \quad (29)$$

Beyond this value of  $R$ , the performance constraint cannot be satisfied and the transmission capacity of the network is zero.

### C. Random link distances

The analytical results derived in this section can be extended to the case where the distance of each TX-RX link is randomly drawn from a distribution. For ease of exposition, assume that  $R$  takes values in a discrete set  $\mathcal{R} = \{R_1, R_2, \dots, R_M\}$  with probabilities  $p_1, \dots, p_M$ , where  $\sum_{m=1}^M p_m = 1$ . If the

operating frequency has a fixed value  $f_o$ , then, similarly to (26) the throughput density is

$$\tau(\lambda) = \lambda \sum_{m=1}^M p_m \exp \left( -\lambda V_d(R_m, f_o) - \frac{\theta R_m^b a(f_o)^{R_m} W(f_o) \delta f}{P} \right). \quad (30)$$

where, with the notation  $V_d(R_m, f_o)$ , we have emphasized the dependence of  $V_d$  on  $R_m$  and  $f_o$ .

In the case where, for each link distance value  $R_m$ , a different operating frequency  $f_{o,m}$  can be selected, we may divide the original network in  $M$  subnetworks, corresponding to the different values of  $R$ , with densities  $\lambda_1 = \lambda p_1, \dots, \lambda_M = \lambda p_M$  (where  $\lambda = \sum_{m=1}^M \lambda_m$ ). Then, the total network throughput density can be found by adding the individual throughput densities of the  $M$  subnetworks, i.e.,

$$\tau(\lambda) = \lambda \sum_{m=1}^M p_m \exp \left( -\lambda p_m V_d(R_m, f_{o,m}) - \frac{\theta R_m^b a(f_{o,m})^{R_m} W(f_{o,m}) \delta f}{P} \right). \quad (31)$$

## IV. NUMERICAL RESULTS

In this section, we present a numerical example for the parameter set  $d = 3$ ,  $b = 1.5$ ,  $\theta = 10$  dB,  $R = 1000$  m and  $P/\delta f = 110$  dB re  $\mu\text{Pa}/\text{Hz}$ . Moreover, we perform Monte Carlo simulations over 20000 network topologies with 10 different fading realizations per topology, in order to verify the validity of the expressions derived in Section III.

We first consider the interference-limited case. In Fig. 1,  $P_{s,i}$  in (6) is plotted as a function of  $a$  for a TX density  $\lambda = 0.01$  nodes/km<sup>3</sup>.  $P_{s,i}$  is an increasing function of  $a$  and, for large  $a$ , slowly approaches  $e^{-\lambda c_3 R^3} \approx 0.96$ , as predicted in Proposition 2. Since  $a(f_o)$  is an increasing function of  $f_o$  (see footnote 2), increasing the carrier frequency  $f_o$  improves the interference-limited success probability. The bounds obtained from (22) for  $N = 2, 4$  are also plotted for comparison and are shown to be reasonably tight. Moreover, for  $a > 10$  dB/km (corresponding to  $f_o = 35$  kHz), the approximation (21) is within 7% of the exact  $P_{s,i}$ .

Since  $P_{s,i}$  increases in  $f_o$ , (26) and (27) imply the existence of a throughput-optimal frequency: as  $f_o$  (or  $a(f_o)$ ) increases,  $V_d$  decreases, i.e., the larger absorption factor allows for a denser packing of transmissions. However, the useful signal power also suffers from absorption, which is reflected in the reduction of the SNR  $P a(f_o)^{-R} R^{-b} / (W(f_o) \delta f)$ .<sup>4</sup> In Fig. 2,  $\tau_o$  (27) and  $c_{0.05}$  (28), optimized over the operating frequency  $f_o$ , are plotted as functions of  $R$ . The respective optimal frequencies are shown in Fig. 3. For comparison, we also plot  $\tau_o$  evaluated at the frequencies which maximize the SNR at each  $R$ . Note that the throughput-optimal frequency is significantly higher for moderate transmission distances, e.g., it is 65 kHz at  $R = 1000$  m, compared to the SNR-optimal value of 20 kHz. The respective throughput, as seen

<sup>4</sup>The increase in  $f_o$  also results in a small decrease of the noise power  $W(f_o)$  [9], but the absorption effect dominates.

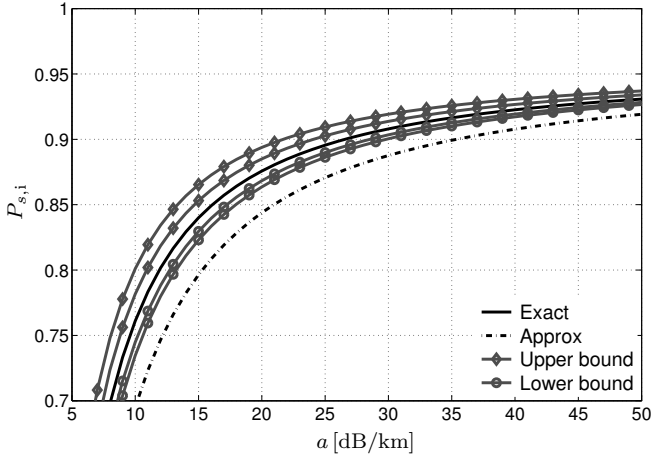


Figure 1.  $P_{s,i}$  vs.  $a$  [dB/km] for  $\lambda = 0.01$  nodes/km<sup>3</sup> and  $\theta = 10$  dB. The exact curve is obtained by numerically evaluating (6) and the approximation corresponds to (21). The outer and inner bounds are obtained by setting  $N = 2$  and  $N = 4$  in (22), respectively. ( $b = 1.5$ ,  $d = 3$ ,  $R = 1000$  m.)

in Fig. 2, is about seven times larger. As the transmission distance increases, the network becomes noise-limited and the gap between the different curves narrows. At  $R \approx 3.5$  km, the frequency which maximizes  $c_{0.05}$  is equal to the frequency which maximizes the SNR. Beyond this value of  $R$ , obtained by (29), the constraint  $1 - \varepsilon = 0.95$  on the success probability is no longer feasible (i.e., the nominator of (28) is negative for any value of  $f_o$ ) and the transmission capacity is zero.

## V. MODEL VALIDATION WITH RAY TRACING SIMULATIONS

### A. Section outline and methodology

In this section, we compare the theoretical results derived in Section III against the outcome of network simulations, where acoustic propagation is modeled using the Bellhop ray tracing software [19]. In contrast to the heuristic model of Section II, Bellhop accurately simulates real acoustic propagation, allowing us to capture the impact of important environmental parameters such as the sound speed profile (SSP) on the network performance.

Network simulations with Bellhop are a very time-costly affair, if the channel from each TX to the RX is computed anew for every realization of the TX PPP and the SSP. Indicatively, obtaining in this manner a throughput curve such as those shown in Fig. 6 may take three to four weeks on a 2.93 GHz Intel Core2 Duo E7500-based machine. To bypass this difficulty, we construct *offline* a channel database for a range of TX-RX distances (in small increments) and different SSPs; then, for each realization of the TX PPP and the SSP, we quantize each TX position to the closest database distance. The impact of quantization on the accuracy of the simulations is negligible but the computational savings are very significant, e.g., an initial four days is required to set up the database for the particular simulation scenario considered in this section, after which producing each simulation curve in Fig. 6 takes less than ten hours.

The channel database is not only useful in speeding up the Bellhop network simulations, but also in enabling the comparison between the theoretical results of Section III and

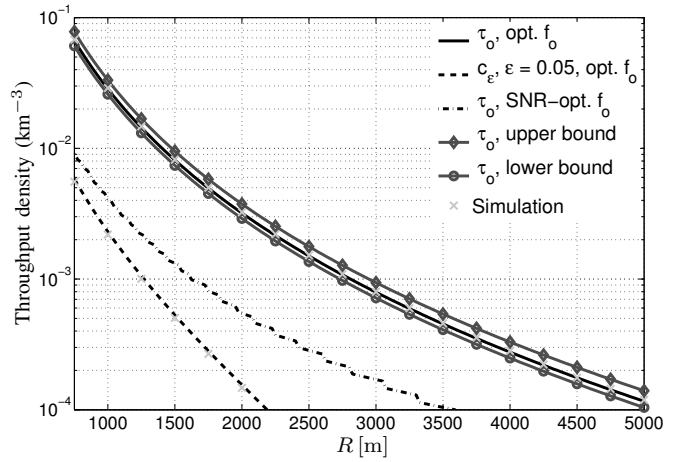


Figure 2. The curves “ $\tau_o$ , opt.  $f_o$ ”, and “ $c_\varepsilon$ ,  $\varepsilon = 0.05$ , opt.  $f_o$ ” correspond to (27) and (28), optimized over  $f_o$  for each  $R$ . “ $\tau_o$ , SNR-opt.  $f_o$ ” is obtained by setting in (27), for each  $R$ , the  $f_o$  which maximizes the received SNR. Note that imposing a constraint  $1 - \varepsilon = 0.95$  on  $P_s$  results in a less dense UW network and in a throughput loss. The upper and lower bound curves are obtained by setting  $N = 2$  in (22) and optimizing the respective expressions over  $f_o$ . ( $P/\delta f = 110$  dB re  $\mu\text{Pa}/\text{Hz}$ ,  $b = 1.5$ ,  $d = 3$ .)

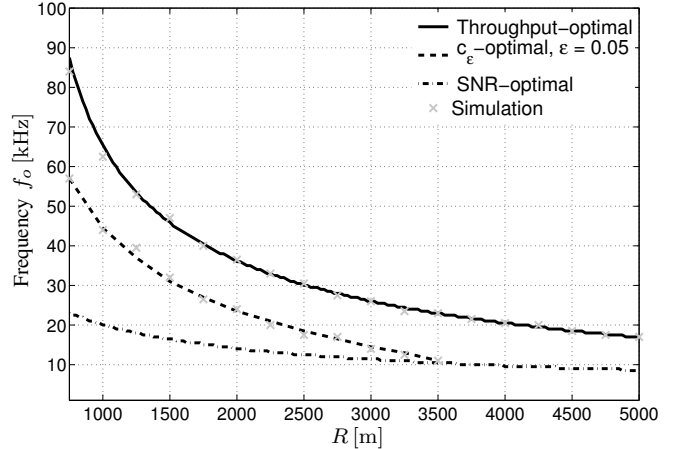


Figure 3. Optimal operating frequencies vs.  $R$ , corresponding to Fig. 2. Boosting the frequency for moderate transmission distances increases the throughput density, as it results in the absorption of interfering signals, e.g., for  $R = 1000$  m, the throughput-optimal  $f_o$  is 65 kHz as opposed to the SNR-optimal  $f_o$  which is 20 kHz. As seen in Fig. 2, this corresponds to a seven-fold throughput increase ( $P/\delta f = 110$  dB re  $\mu\text{Pa}/\text{Hz}$ ,  $b = 1.5$ ,  $d = 3$ .)

the network simulation results. In particular, we employ the database in order to calculate the average channel gain (over different SSPs) at each distance  $R$ , and then use a curve-fitting procedure, in order to best match it to the empirical gain  $R^{-b}a(f)^{-R}$ , by varying the spreading-loss exponent  $b$ . The tuned  $b$  is substituted in the expressions of Section III to compute the theoretical network throughput, which is then compared with the outcome of the Bellhop network simulation.

In the rest of this section, we present in detail the steps outlined above and the comparison between theoretical and simulation results.

### B. Simulation scenario and channel gain database

The chosen location of the Bellhop simulations is south of the Elba island in the Tyrrhenian sea, with coordinates

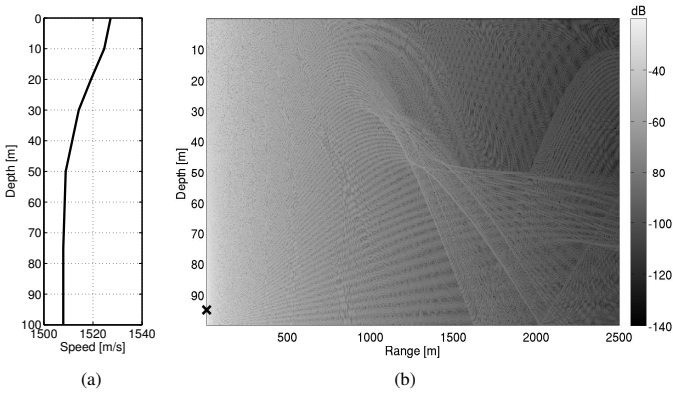


Figure 4. (a) Average May SSP taken from the WOD 2009 database, for a 100 m-deep location in the Tyrrhenian sea at  $(10.5^\circ\text{E}, 42.5^\circ\text{N})$ . (b) Channel power gain in dB obtained using Bellhop. The TX (marked by a cross on the left side of the picture) is at a depth of 95 m and the frequency is  $f_o = 50$  kHz. Darker shades of grey correspond to a weaker signal.

$(10.5^\circ\text{E}, 42.5^\circ\text{N})$ . The sea floor is at a depth of 100 m, and the nodes are all situated at a depth of 95 m, which is a deployment typical of a bottom-monitoring network. (However, such a planar deployment is also common for floating devices that monitor environmental parameters at smaller depths [27].) The TXs are located within a disc of radius 5000 m,<sup>5</sup> and the RX of interest is placed at its center, with its respective TX at a distance  $R$  and an arbitrary orientation.

We first create a baseline configuration file for Bellhop which contains all the simulation and environmental parameters. The sea surface and bottom are approximated as flat, the geo-acoustic parameters of the bottom sediments are taken from the Deck41 database [28], and the average May SSP from the 2009 World Ocean Database (WOD) [29], shown in Fig. 4(a), is selected. We set the number of rays to be traced to 120000,<sup>6</sup> with angles of departure from the TX ranging from  $-89^\circ$  to  $+89^\circ$ . Based on the path that it follows, each ray has a given amplitude and phase at the RX, and the total received power is computed by taking the squared norm of the subset of rays which carry significant power to the RX position. (More details on how this set is determined can be found in [30, Ch. 3, Section 3.5.2].) In Fig. 4(b), a snapshot of the channel gain, i.e., the ratio of the total received power over the TX power, throughout the water column is depicted. The mild downward refraction is due to the shape of the SSP in Fig. 4(a).

For a fixed SSP and RX location, the channel gain for a TX at distance  $R$  is deterministic, and does not depend on the TX orientation due to the circular symmetry which results from the flat sea surface and bottom. We generate an ensemble of 5000 channel gain realizations by simultaneously adding small displacements to the SSP at depths 0, 10, 20, 30, 50, 75 and 100 m (standard depths in WOD [29]), which are drawn independently and uniformly from the interval  $[-4, +4]$  m/s.<sup>7</sup>

<sup>5</sup>For the range of transmission distances in this section, the interference from nodes farther than 5000 m can be neglected.

<sup>6</sup>This is more than twice the minimum number of rays required by Bellhop to achieve satisfactory accuracy.

<sup>7</sup>Such displacements were observed during the SubNet'09 trials in the Tyrrhenian sea [31]. Note that the small displacement range preserves the downward-refractive behavior of the channel.

A database of channel gain realizations is created by repeating this procedure for all TX distances from 10 m to 5000 m in increments of 10 m. The role of the database is to speed up the Bellhop network simulations described in Section V-D. Moreover, it is used to fit the empirical channel gain of the Urick model to the average simulated gain, by appropriately tuning  $b$ , which is described in the following.

### C. Tuning the spreading-loss exponent $b$ of the Urick model

The comparison between the theoretical and simulated throughput is meaningful only if, for a given  $R$ , the empirical gain  $R^{-b}a(f)^{-R}$  of the Urick model is comparable to the one simulated with Bellhop. In Fig. 5, the simulated average gain (obtained by taking the average of the channel gain over all SSP realizations for each  $R$ ) is plotted vs.  $R$  for  $f = 20, 50$  and  $90$  kHz. As expected, the curves are steeper as  $f$  increases, due to the larger signal absorption. The average gain obtained with the Urick model is also plotted vs.  $R$ , where, for each frequency,  $b$  is selected such that the Urick gain fits the simulated one in the least squares sense.<sup>8</sup> The small discrepancies observed in each curve pair are due to the inability of the Urick model to capture specific environmental effects, e.g., the strong insonification of the sea bottom due to the downward refraction, or the local interference patterns originated by the interaction of the direct propagation path with surface bouncing paths carrying comparable power. For all frequencies, we note that  $b$  is larger than the “practical spreading factor” 1.5 introduced in [9] and used in many shallow water network simulation studies, which is in accordance with the statement in [10, p. 102].

### D. Bellhop network simulations and comparison with theoretical results

For a given PPP density  $\lambda$  and typical TX-RX link distance  $R$ , the success probability at RX, defined in (3), is evaluated by comparing the SINR with the threshold  $\theta = 10$  dB for 4000 realizations of the TX PPP, and 5000 realizations of the SSP generated as described in Section V-B. For each realization of the TX PPP and the SSP, the distance of each interfering TX from RX is quantized with a precision of 10 m, and the respective database entry is invoked to determine the channel gain between that TX and RX. In this manner, the channel gain database can be invoked repeatedly across different topology and SSP realizations. The simulated network throughput is calculated as the product of the TX density and the simulated success probability. The theoretical network throughput is determined by (26), employing the fitted value of  $b$ , obtained as described in Section V-C. As in Section IV, we set  $P/\delta f = 110$  dB re  $\mu\text{Pa}/\text{Hz}$ . We consider  $R$  and  $f_o$  in the ranges 800 – 1500 m, 20 – 90 kHz, respectively.

In Fig. 6, the theoretical and simulated throughput densities are plotted vs.  $\lambda$  for  $R = 1000$  m and  $f_o = 20, 50$  kHz. The shape of the curves is typical of random-access (ALOHA)

<sup>8</sup>Whereas  $a(f)$  is an empirical function precisely determined in the literature [9] and simulation software [19], existing guidelines for selecting the value of  $b$  are rather vague. We therefore chose to tune  $b$  to achieve the fit and left  $a(f)$  unchanged.

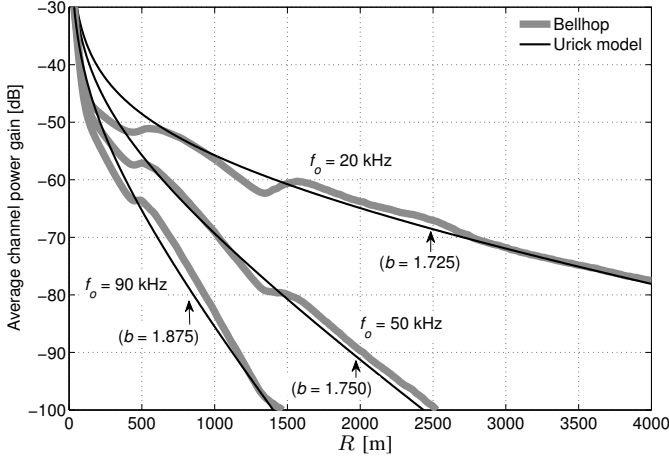


Figure 5. Average power gain in dB vs.  $R$  for  $f_o = 20, 50, 90$  kHz, using Bellhop simulations and the Urick model. The Urick curves are obtained by least-squares fitting with the simulation results. The “valleys” observed in the vicinity of 400 m and 1300 m are due to the destructive interference between direct ray arrivals, surface bounces and bottom bounces, which occurs at these distances.

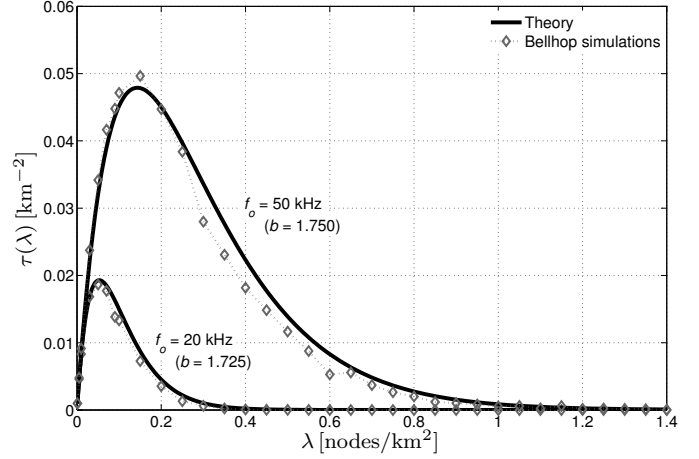


Figure 6. Theoretical and simulated throughput density vs.  $\lambda$  for  $f_o = 20, 50$  kHz at  $R = 1000$  m. The Bellhop simulation results match the theoretical throughput satisfactorily, for the fitted values of  $b$ .

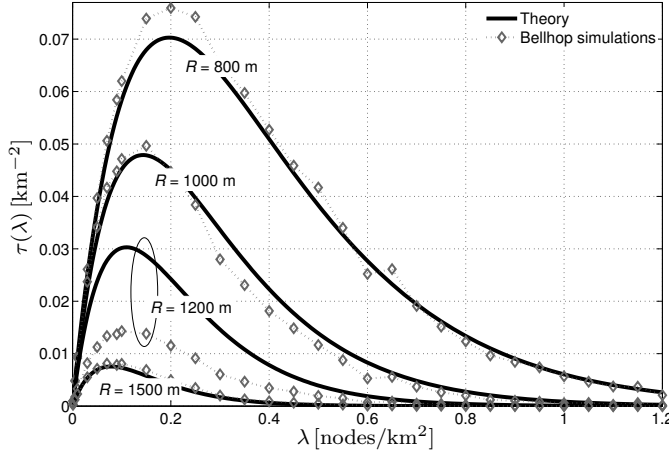


Figure 7. Theoretical and simulated throughput density vs.  $\lambda$  for  $f_o = 50$  kHz and different values of  $R$ . The maximum throughput increases for decreasing  $R$  as attenuation of the useful signal decreases. The match between the simulation and theoretical results (obtained for  $b = 1.750$ ) is good at  $R = 800, 1000, 1500$  m, while at  $R = 1200$  m, the theory overestimates the simulated throughput.

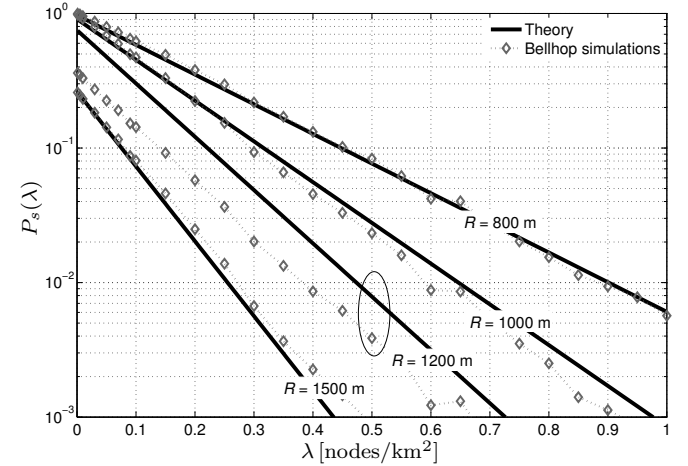


Figure 8. Theoretical and simulated success probability vs.  $\lambda$  corresponding to Fig. 7. The Bellhop simulation results are in good accordance with the theoretical results, except for  $R = 1200$  m where the theory overestimates  $P_s$ .

systems, i.e., for small  $\lambda$ ,  $\tau(\lambda)$  increases linearly in  $\lambda$ , while, for large  $\lambda$ , it decreases exponentially, and the maximum occurs at the density  $\lambda_o = V_d^{-1}$ . We observe a very good match between theoretical and simulation results, with only a slight overestimation of the throughput density by the theory in the descending portion of the curves.

In Figs. 7 and 8, the theoretical/simulated throughput densities and respective success probabilities are plotted vs.  $\lambda$  for  $f_o = 50$  kHz and different  $R$ . The plots confirm the overall agreement between theory and simulation, except in the case of  $R = 1200$  m, where the theory overestimates the simulated success probability and the throughput. These results are explained in Fig. 9, where the histogram of the simulated gain is plotted for  $R = 1000, 1200, 1500$  m. The exponential distribution provides a satisfactory fit to the histogram for  $R = 1500$  m. In the case of  $R = 1000$  m, the peaks in the vicinity of  $40 \times 10^{-9}$  disagree with the exponential model. Yet,

since the peaks occur at gain values *larger* than  $\theta W(f_o) \delta f / P$ , they do not affect the noise-limited performance of the typical link, thus the simulated success probability and throughput follow closely the theoretical ones, as seen in Figs. 7 and 8. In contrast, for  $R = 1200$  m, the peak occurs at  $10 \times 10^{-9}$  which is slightly less than  $\theta W(f_o) \delta f / P$ , resulting in a smaller success probability and throughput density. This “shadowing” effect is attributed to destructive interference between the direct arrivals, the bottom bounces and the surface bounces occurring in the range 1200 – 1400 m, as also shown in Fig. 5. The main conclusions from these observations are that (a) the match between theory and simulation is not crucially dependent on the exponential fading assumption, provided that the typical link does not experience shadowing, and (b) even when this is the case (as for  $R = 1200$  m), the discrepancy is *independent* of the TX density, hence the maximum simulated and theoretical throughput still occur at the same TX density, as shown in Fig. 7.

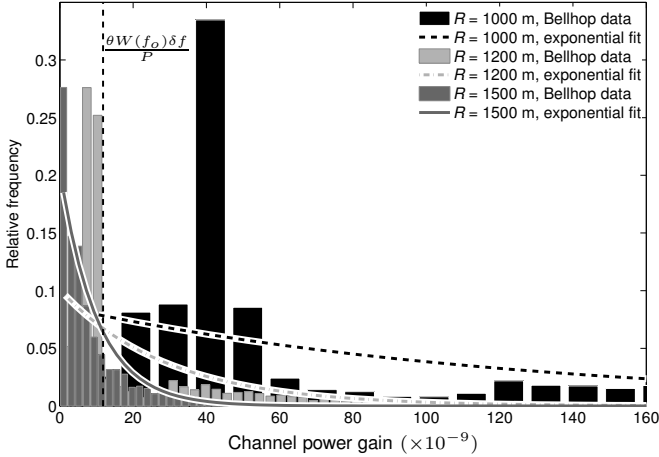


Figure 9. Relative frequency histogram of the Bellhop simulated channel gain for  $R = 1200, 1000, 1500$  m at  $f_o = 50$  kHz. For all values of  $R$ , an exponential distribution has been fitted to the histograms. The fit is good for  $R = 1500$  m but unsatisfactory for  $R = 1000, 1200$  m due to the presence of peaks in the vicinity of  $40 \times 10^{-9}$  and  $10 \times 10^{-9}$ , respectively. For  $R = 1200$  m, these peaks are lower than the value  $\theta W(f_o)\delta f/P \approx 11 \times 10^{-9}$ , which yields a success probability smaller than the theoretical one, as seen in Fig. 8.

The results presented so far demonstrate that the theory accurately predicts the simulated throughput for a wide range of parameters, provided that  $b$  is appropriately selected. Therefore, a semi-analytic method can be followed in order to compute the network throughput for given  $R$ ,  $\lambda$  and  $f_o$ , in the realistic acoustic propagation environment of Bellhop, consisting of the following steps: (a) constructing the database of channel realizations for a *single* TX-RX link as in Section V-B, (b) selecting  $b$  using said database, as described in Section V-C, and (c) calculating  $\tau(\lambda)$  from (26) for the selected  $b$ . As an indicative example, this procedure is applied to select the throughput-optimal  $f_o$  for  $R = 1000$  m. In Fig. 10,  $\tau(\lambda)$  is plotted vs.  $\lambda$  for different frequencies in the range 20 – 70 kHz. The maximum throughput is shown to be achieved at  $\lambda^* = 0.15$  nodes/km<sup>2</sup> and  $f_o^* = 50$  kHz, which is confirmed independently by the network simulations with Bellhop. The discrepancies between theoretical and simulated throughput are due to channel mismatch issues similar to those described in the previous paragraph, which, nevertheless, do not impact the optimal operating point  $(\lambda^*, f_o^*)$  yielded by the semi-analytical procedure.

## VI. CONCLUDING REMARKS

We proposed an analytical framework to evaluate the throughput of UW networks, taking into account the characteristics of the UW channel and the dependence of the interference power on the TX locations. The analysis is based on the assumptions that the TX locations are drawn from a PPP, a model that has been employed widely for the performance analysis of wireless radio networks, and on an empirical underwater channel model used in many existing works to date. We obtained easy-to-calculate expressions and bounds to the success probability, the throughput density and the transmission capacity, which capture the effect of salient parameters such as the spreading-loss exponent and the

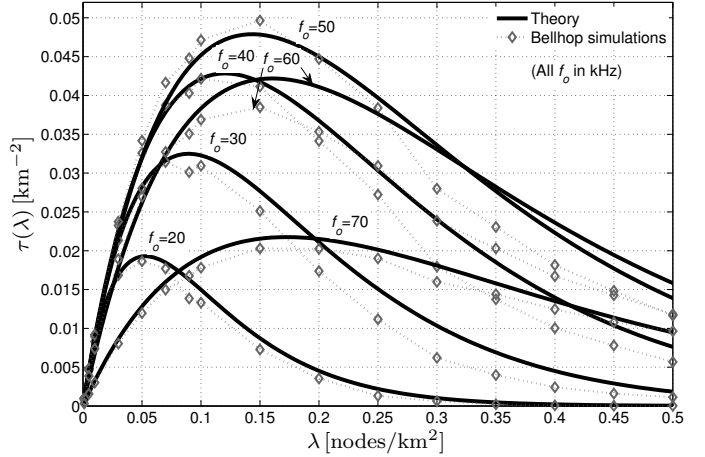


Figure 10. Theoretical and simulated throughput density vs.  $\lambda$  for several values of  $f_o$  (in kHz) at  $R = 1000$  m. For each  $f_o$ ,  $b$  is selected as described in Section V-C. The maximum theoretical throughput density occurs at  $\lambda \approx 0.15$  nodes/km<sup>2</sup> and  $f_o = 50$  kHz, which is confirmed independently by the network Bellhop simulation.

carrier frequency. Numerical results showed that, for moderate transmission distances, boosting the carrier frequency yields a significant throughput gain, since the benefit of the absorption of interfering signals outweighs the loss due to the absorption of the intended signal.

The analysis was validated with extensive simulations for a shallow-water network scenario. Using curve-fitting, the spreading-loss exponent in the empirical model was selected to achieve the best match between the mean empirical and simulated received power for a single TX-RX link. The obtained spreading-loss exponent was then substituted in the theoretical expressions, which predicted the simulated throughput with satisfactory accuracy. Following this semi-analytical approach instead of performing a full-blown Bellhop network simulation results in a reduction of the simulation time from several weeks to just a few hours.

Although the simulations were performed at a particular location, our approach can be applied to other shallow-water locations, as long as  $b$  is fitted appropriately. Moreover, the case of 3D networks can be accommodated, provided that a channel database that also includes various depths is created. In general environments, e.g., deep-water, a channel modeling study is required to determine the statistics of the received power. If such information is available, the analysis of Section III can in principle be modified to accommodate other empirical models and fading statistics. The extension of the results presented in the paper to a wideband channel or to the multi-hop scenario is left for future investigation.

## REFERENCES

- [1] M. Chitre, S. Shahabudeen, and M. Stojanovic, "Underwater acoustic communications and networking: recent advances and future challenges," *Marine Tech. Soc. Journal*, vol. 42, no. 1, pp. 103–116, Spring 2008.
- [2] J. Rice, "SeaWeb acoustic communication and navigation networks," in *Proc. of IACM UAM*, Heraklion, Greece, 2005.
- [3] J. G. Proakis, E. M. Sozer, J. A. Rice, and M. Stojanovic, "Shallow water acoustic networks," *IEEE Commun. Mag.*, vol. 39, no. 11, pp. 114–119, Nov. 2001.

- [4] Z. Peng, J.-H. Cui, B. Wang, K. Ball, and L. Freitag, "An underwater network testbed: design, implementation and measurement," in *Proc. of ACM WUWNet*, Montréal, Canada, Sep. 2007.
- [5] D. Pompili and I. Akyildiz, "Overview of networking protocols for underwater wireless communications," *IEEE Commun. Mag.*, vol. 47, no. 1, pp. 97–102, Jan. 2009.
- [6] H. Nguyen, S.-Y. Shin, and S.-H. Park, "State-of-the-art in MAC protocols for underwater acoustics sensor networks," in *Emerging Directions in Embedded and Ubiquitous Computing*, ser. Lecture Notes in Computer Science. Springer, 2007, vol. 4809, pp. 482–493.
- [7] F. Guerra, P. Casari, and M. Zorzi, "World Ocean Simulation System (WOSS): a simulation tool for underwater networks with realistic propagation modeling," in *Proc. of ACM WUWNet*, Berkeley, CA, Nov. 2009.
- [8] M. Zorzi, P. Casari, N. Baldo, and A. F. Harris III, "Energy-efficient routing schemes for underwater acoustic networks," *IEEE J. Sel. Areas Commun.*, vol. 26, no. 9, pp. 1754–1766, Dec. 2008.
- [9] M. Stojanovic, "On the relationship between capacity and distance in an underwater acoustic communication channel," *ACM Mobile Comput. and Commun. Review*, vol. 11, no. 4, pp. 34–43, Oct. 2007.
- [10] R. J. Urlick, *Principles of Underwater Sound*. New York: McGraw-Hill, 1975.
- [11] P. Casari, M. Stojanovic, and M. Zorzi, "Exploiting the bandwidth–distance relationship in underwater acoustic networks," in *Proc. of MTS/IEEE Oceans*, Vancouver, Canada, Sep. 2007.
- [12] M. Stojanovic, "Frequency reuse underwater: capacity of an acoustic cellular network," in *Proc. of ACM WUWNet*, Montréal, Canada, Sep. 2007.
- [13] J. Partan, J. Kurose, and B. Levine, "A survey of practical issues in underwater networks," in *Proc. of ACM WUWNet*, Los Angeles, CA, Sep. 2006.
- [14] D. Lucani, M. Médard, and M. Stojanovic, "Capacity scaling laws for underwater networks," in *Proc. of 42<sup>nd</sup> Asilomar Conf. on Signals, Systems and Computers*, Pacific Grove, CA, Oct. 2008.
- [15] W. Shin, D. E. Lucani, M. Médard, M. Stojanovic, and V. Tarokh, "Multi-hop routing is order-optimal in underwater extended networks," in *Proc. of IEEE ISIT*, Austin, TX, Jun. 2010.
- [16] M. Haenggi, J. G. Andrews, F. Baccelli, O. Dousse, and M. Franceschetti, "Stochastic geometry and random graphs for the analysis and design of wireless networks," *IEEE J. Sel. Areas Commun.*, vol. 27, no. 7, pp. 1029–1046, Sep. 2009.
- [17] S. Weber and J. G. Andrews, *Transmission Capacity of Wireless Networks*, ser. Foundations and Trends in Networking. NOW, 2012, vol. 5.
- [18] J. G. Andrews, S. Weber, M. Kountouris, and M. Haenggi, "Random access transport capacity," *IEEE Transactions on Wireless Communications*, vol. 9, no. 6, pp. 2101–2111, Jun. 2010.
- [19] M. Porter *et al.*, "Bellhop code." [Online]. Available: <http://oalib.hlsresearch.com/Rays/index.html>
- [20] M. Chitre, "A high-frequency warm shallow water acoustic communications channel model and measurements," *J. Acoust. Soc. Am.*, vol. 122, no. 5, pp. 2580–2586, May 2007.
- [21] A. Porto and M. Stojanovic, "Optimizing the transmission range in an underwater acoustic network," in *Proc. of MTS/IEEE OCEANS*, Vancouver, Canada, Oct. 2007.
- [22] U. Lee, P. Wang, Y. Noh, F. M. L. Vieira, M. Gerla, and J.-H. Cui, "Pressure routing for underwater sensor networks," in *Proc. of IEEE INFOCOM*, San Diego, CA, Mar. 2010.
- [23] Z. Zhou, Z. Peng, J.-H. Cui, and Z. Jiang, "Handling triple hidden terminal problems for multi-channel MAC in long-delay underwater sensor networks," in *Proc. of IEEE INFOCOM*, San Diego, CA, Mar. 2010.
- [24] F. Baccelli and B. Błaszczyszyn, *Stochastic Geometry and Wireless Networks*, ser. Foundations and Trends in Networking. NOW, 2009, vol. 1.
- [25] I. S. Gradshteyn and I. M. Ryzhik, *Table of integrals, series and products*, 7th ed. Academic Press, 2007.
- [26] R. M. Corless, G. H. Gonnet, D. E. G. Hare, D. J. Jeffrey, and D. E. Knuth, "On the Lambert W function," *Advances in Computational Mathematics*, vol. 5, pp. 329–359, 1996.
- [27] L. Freitag, M. Grund, S. Singh, and M. Johnson, "Acoustic communication in very shallow water: Results from the 1999 AUV Fest," in *Proc. of MTS/IEEE Oceans*, Providence, RI, Sep. 2000.
- [28] "National Geophysical Data Center, seafloor surficial sediment descriptions." [Online]. Available: <http://www.ngdc.noaa.gov/mgg/geology/deck41.html>
- [29] "World ocean database." [Online]. Available: [http://www.nodc.noaa.gov/OC5/WOD09/pr\\_wod09.html](http://www.nodc.noaa.gov/OC5/WOD09/pr_wod09.html)
- [30] F. Jensen, W. Kuperman, M. Porter, and H. Schmidt, *Computational Ocean Acoustics*, 2nd ed. New York: Springer, 2011.
- [31] S. Azad, P. Casari, C. Petrioli, R. Petrocchia, and M. Zorzi, "On the impact of the environment on MAC and routing in shallow water scenarios," in *Proc. of IEEE/OES Oceans*, Santander, Spain, Jun. 2011.



**Kostas Stamatou** [M'09] received his Diploma in Electrical and Computer Engineering from the National Technical University of Athens in 2000, and the MSc and PhD degrees in Electrical Engineering in 2004 and 2009, respectively, from the University of California San Diego. From 2009 to 2010, he was a post-doctoral scholar in the Department of Electrical Engineering at the University of Notre Dame, South Bend, Indiana, and from 2010 to 2012, he held a research appointment at the Department of Information Engineering at the University of Padova, Italy. He is currently a research associate at the Intelligent Energy group of CTTC, Barcelona. His research interests lie in the general areas of communication theory, stochastic geometry and random networks, and energy harvesting systems.



**Paolo Casari** [M'08] received the PhD in Information Engineering in 2008 at the University of Padova, Italy, where he is currently a postdoctoral research fellow. He has been actively researching cross-layer protocol design for MIMO ad hoc networks and wireless sensor networks. After spending a period at the Massachusetts Institute of Technology in 2007, he started working on underwater acoustic networks, which is currently his main focus. He has been the technical manager of the Italian projects WISE-WAI and NAUTILUS, and is currently involved in several efforts funded within the European Community's FP7 program, and related to underwater acoustic networking. He served in the organizing committee of several conferences, and has been guest editor for the Hindawi Journal of Electronics and Computer Engineering special issue on "Underwater Communications and Networking." His research interests include many aspects of underwater communications, such as channel modeling, network performance evaluation, cross-layer protocol design and at-sea experiments.



**Michele Zorzi** [F'07] received his Laurea and PhD degrees in electrical engineering from the University of Padova in 1990 and 1994, respectively. During academic year 1992-1993 he was on leave at UCSD, attending graduate courses and doing research on multiple access in mobile radio networks. In 1993 he joined the faculty of the Dipartimento di Elettronica e Informazione, Politecnico di Milano, Italy. After spending three years with the Center for Wireless Communications at UCSD, in 1998 he joined the School of Engineering of the University of Ferrara, Italy, where he became a professor in 2000. Since November 2003 he has been on the faculty of the Information Engineering Department at the University of Padova. His present research interests include performance evaluation in mobile communications systems, random access in mobile radio networks, ad hoc and sensor networks, energy constrained communications protocols, and underwater communications and networking. He was Editor-In-Chief of IEEE WIRELESS COMMUNICATIONS from 2003 to 2005 and Editor-In-Chief of the IEEE TRANSACTIONS ON COMMUNICATIONS from 2008 to 2011, and serves on the Editorial Board of the Wiley JOURNAL OF WIRELESS COMMUNICATIONS AND MOBILE COMPUTING. He was also guest editor for special issues in IEEE PERSONAL COMMUNICATIONS ("Energy Management in Personal Communications Systems") and IEEE JOURNAL ON SELECTED AREAS IN COMMUNICATIONS ("Multimedia Network Radios" and "Underwater Wireless Communications and Networking"). He served as a Member-at-Large of the Board of Governors of the IEEE Communications Society from 2009 to 2011.